A Decentralized Secondary Frequency Restoration Control with Local Current for Island Cascaded-type Microgrids

Shi, Guangze; Han, Hua; Sun, Yao; Ou, Junlan; Guan, Yajuan; Guerrero, Josep M.

Published in:
IEEE Transactions on Power Systems

DOI (link to publication from Publisher):
10.1109/TPWRS.2022.3206341

Publication date:
2023

Document Version
Accepted author manuscript, peer reviewed version

A Decentralized Secondary Frequency Restoration Control with Local Current for Island Cascaded-type Microgrids

Guangze Shi, Hua Han, Yao Sun, Member, IEEE, Junlan Ou,Yajuan Guan, Member, IEEE, and Josep M. Guerrero, Fellow, IEEE

***Abstract*—Frequency regulation is important for obtaining higher power supply quality. To our best knowledge, there is no decentralized frequency restoration method for cascaded-type microgrid. This paper proposes a decentralized second frequency control for the cascaded-type microgrid. It only relies on local information to achieve frequency restoration and average power sharing. In addition, the proposed control is suitable for loads with different characteristics. Based on the singularity theory, we provide the control algorithm convergence analysis and control coefficient selection. Finally, the real-time simulation results conducted by RTLAB verify the feasibility of the proposed method.**

***Keywords*—Second Frequency Regulation, Island Cascaded-type Microgrid, Power Sharing**

I. INTRODUCTION

The world energy structure is going through a period of irreversible change. Renewable energy resource plays a more and more important role in this transition [1]. But the intermittent characteristic introduces challenges for the power stability and quality [2]. Microgrid as an effective solution is able to coordinate the generation resources and loads. According to the interfacing converters connection structure, microgrids can be divided into two types, paralleled connected or cascaded connected.

Evolved from the power system, the paralleled-type microgrid becomes the researched mainstream. The most commonly used approach, droop control [3], can obtain power sharing among generation units and improve system reliability. Based on droop control, many decentralized control methods are proposed for PV, energy storage systems, and so on [4, 5]. But the droop control sacrifices power quality like frequency/voltage deviation. The secondary restoration control provides a promising solution for improving the power quality of the microgrid [6]. It can not only restore the voltage/frequency deviation caused by the droop control but also improve power sharing precision. Thus, secondary restoration control has an indispensable position in the field of microgrid control. The existing secondary restoration control methods are categorized into two types: communication-based and non-communication-based.

According to communication topology, as shown in Fig. 1, the communication-based methods can be divided into three parts: centralized control, master-slave control, and distributed control. The centralized secondary control [7] relies on a central controller to send instructions to each local controller. These control approaches can achieve accurate voltage/frequency restoration and power sharing. However, due to the high dependence on high-bandwidth communication and centralized controller, the reliability of microgrid will decrease. Moreover, the computation load and the cost of communication will increase with the number of cascaded units increasing. For master-slave control [8], the master unit controller can provide instructions to slaver units instead of the centralized controller. To avoid the reliability reduction, a maximum power loading factor control [9] is proposed with automatic selection of the master unit. But this method has a weak ability to deal with communication disturbance and failure. This promotes the wide use of distributed control in microgrids, which can coordinate the generation resources by using neighbor information. Authors in [10] proposed a secondary control to restore system frequency/voltage through a distributed consensus algorithm. In [11], the authors use distributed consensus algorithms to estimate global average frequency/voltage, which is used as feedback to achieve restoration objectives. Apart from good performance, the distributed control has merits in lower communication dependence over centralized control and master-slaver control. The distributed control relies on low-bandwidth communication, which greatly reduces the communication requirements and costs compared with centralized control.

However, these three types of communication-based methods still rely on the communications links to exchange information. So the security and stability of the microgrids will be threatened by communication delay, disturbance, and failure. To further reduce communication dependency, some researchers have developed decentralized secondary control, which only relies on local information. Reference [12] proposes a self-optimizing control strategy, which uses a low-pass filter to achieve restoration and optimization objectives. But the accuracy of the frequency restoration is not precise. Combining the function of the low-pass filter, a secondary control [13] that switches between two configurations is proposed for accurate frequency restoration in steady state. But the switch failure and detection disturbance will threaten the stable operation of the microgrid.

This work was supported in part by the science and technology innovation Program of Hunan Province under Grant 2020RC4002, the National Science Fund for Distinguished Young Scholars under Grant 62125308, and the National Natural Science Foundation of China under Grant 52177205 . (*Corresponding author: Yao Sun*.)

G. Shi, H. Han, J. Ou and Y. Sun are with the School of Automation, Central South University and the Hunan Provincial Key Laboratory of Power Electronics Equipment and Gird, Changsha 410083, China (e-mail: 16414986@qq.com, hua_han@126.com, yaosun@csu.edu.cn, junlan@csu.edu.cn).

Y. Guan and J. M. Guerrero are are with the Department of Energy Technology, Aalborg University, 9220 Aalborg (e-mail: ygu@et.aau.dk; joz@et.aau.dk).

This article has been accepted for publication in IEEE Transactions on Power Systems. This is the author's version which has not been fully edited and content may change prior to final publication. Citation information: DOI 10.1109/TPWRS.2022.3206341

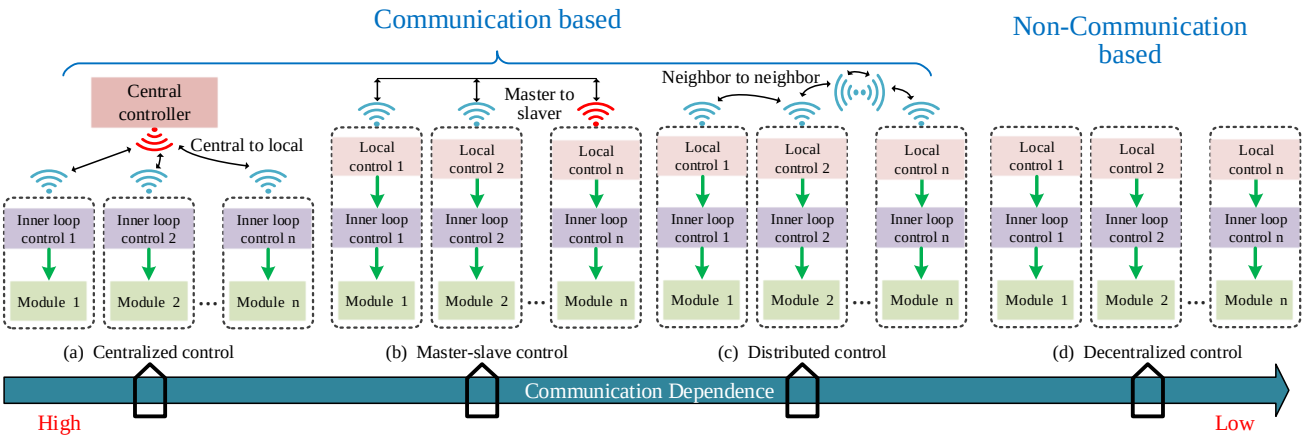

Fig.1 Secondary control categories with communication topologies

Table I State-of-art of previous frequency restoration strategies

Ref.	Control Mechanism		Control Type	Communication Burden	Application (O: Original E: Expandable)	Limitation
[7]	The controllable micro source is in charge of frequency restoration by using load frequency.		Centralized	High	Paralleled-type Microgrid (O) Cascaded-type Microgrid (E)	1. High computational load when DG numbers increase a lot. 2. High dependence of control signal on real-time communication. 3. Low reliability due to communication vulnerability risks and central controller failure.
[24]	Hierarchical control for voltage and frequency regulation				Paralleled-type Microgrid (E) Cascaded-type Microgrid (O)	
[25]	A two-layer coordinated power flow control					
[8]	The DG with largest influence is chosen as the master node for secondary frequency control.		Master-slaver	High	Paralleled-type Microgrid (O) Cascaded-type Microgrid (E)	1. High dependence on real-time communication. 2. Low reliability due to communication vulnerability risks and master failures.
[9]	The master is responsible for frequency restoration and generating a unified reference signal based on maximum power loading factor algorithm for all DGs.					
[10]	Both frequency and voltage restorations are carried out based on distributed consensus-based frequency control method		Distributed	Low	Paralleled-type Microgrid (O) Cascaded-type Microgrid (E)	1. Complex communication network with high cost 2. High dependence of control signal on real-time communication. 3. Low reliability due to multipoint communication failures risks.
[11]	The secondary control variables are designed based on distributed averaging proportional-integral controller					
[26]	A common second frequency control is designed for frequency restoration and power sharing based on distributed control principle.				Paralleled-type Microgrid (E) Cascaded-type Microgrid (O)	
[12]	The secondary control is implemented using a low-pass filter	P-F droop control	Decentralized	Free	Paralleled-type Microgrid (O)	1. Low accuracy of frequency restoration. 2. Without the ability to be directly applied to cascaded type microgrid
[13]		F-P droop control				

In the last few years, the introduction of cascaded-type microgrids promotes the development of microgrids in high/medium voltage fields, especially large-scale photovoltaic power generation [14], energy storage stations [15], and so on. It not only provides a simple and direct way to boost voltage without bulky transformers and complex circuits. [16], but also improve the control flexibility of each unit. However, most of the traditional control [17]-[19] methods that target cascaded converter systems, such as static synchronous compensators (STATCOMs) and motor drives, are implemented by centralized control. When the distributed generations are geographically far apart, the traditional centralized control will no longer be suitable due to the communication burden for acquiring data and transmitting control commands.

Recently, inspired by the droop mechanism in the paralleled-type microgrid, some researchers attempt at using decentralized control as a potential solution. He *et al*. [20] firstly proposed a decentralized control method and introduced the new concept of series-connected-microconverters-based microgrids. Subsequently, [21] proposes an *f-P/Q* method for wider load impedance characteristics application. In addition, a general power factor droop control is proposed to achieve unified control for both

islanded and grid-connected modes [22]. Considering distributed generation characteristics, some specific application scenarios of the cascaded-type microgrid are widely studied. For instance, a decentralized SOC balancing method is designed for battery energy storage systems in [15]. A decentralized mutual damping control for VSGs is proposed to achieve power and frequency oscillation suppression [23]. However, the focus of these methods is frequency synchronization and power sharing, which ignore the frequency offsets.

Thus, secondary frequency control also plays an important role in cascaded-type microgrid operation. Inspired by communication-based methods of paralleled-type microgrid some works have been attempted in cascaded-type microgrid. Based on a centralized controller, a hierarchical control [24] and a two-layer coordinated power flow control [25] are proposed to realize flexible power regulation and ensure the rated voltage and frequency. To improve reliability and reduce communication burden, the authors in [26] propose a secondary frequency control based on distributed consensus. This method uses neighbor-to-neighbor interactions to exchange information. Considering the drawbacks of the aforementioned communication-based methods, investigation on the non-communication-based control methods for frequency restoration in the cascaded-type microgrid is highly required. It is noted that although communication is indispensable for other important functions in practice, like state monitoring, system protection, etc., reducing the dependence on communication for the controller can improve the reliability in the case of communication vulnerability risks. According to [20]-[23], the control design mechanism of the cascaded-type microgrid is quite different from that of the paralleled-type microgrid. In case of following the decentralized secondary control of the paralleled-type microgrid, the characteristics of the series structure are not fully utilized.

To sum up, Table I shows the state-of-art of the existing studies. As shown in Table I, the previous control approaches still meet some limitations including:

1) Although the application of existing communication-based methods (including centralized and distributed methods) for frequency restoration is not limited by the microgrid structure, the drawbacks are obvious, such as high dependence on the communication network and low reliability in terms of communication and master/central controller failure risks.
2) Up to our knowledge, there is no decentralized frequency restoration method for cascaded-type microgrid. Unlike communication-based methods, the decentralized methods for paralleled-type microgrid cannot be extended to cascaded-type microgrid due to the impact of load impedance characteristics over control stability. Moreover, the accuracy of frequency restoration is not accurate enough.

To overcome these limitations, a decentralized second control for the cascaded-type microgrid is proposed. The main characteristic of the series structure is that all resources sharing the same output current. Taking advantage of this feature, each local control can easily acquire the global average frequency from the respective output current. Thus it is very convenient to achieve frequency restoration with high steady-state accuracy and smooth response performance. In addition, a self-tuning modification is designed to eliminate the power sharing errors caused by external disturbance and initial integration error. Moreover, the stability of the proposed control is proved based on singularity theory. Compared with previous studies, the contributions of this paper are summarized as follows

1. **Providing an easy way to acquire global average frequency based on local information.** Compared with communication-based methods, the proposed control is of flexibility in the usage of the same sharing local currents, which is an easy and convenient way to acquire global frequency information.
2. **Proposing a decentralized frequency recovery strategy with improved performance.** The existing frequency restoration methods for cascaded-type microgrid all rely on communication. The proposed method firstly provides an effective way to restore frequency without communication dependency. Compared with decentralized methods, e.t. low-pass filter based methods, the accuracy of frequency restoration is improved.
3. **Designing a self-tuning modification using local information for ensuring average power sharing.** The main drawback of existing decentralized methods is that the external disturbance is easy to destroy the state of power sharing. In this paper, the self-tuning modification is cleverly designed by singular theory to overcome this drawback. As the frequency recovery control and self-tuning modification are in different time scales, the frequencies are restored quickly after every iteration of self-tuning modification. Thus, the self-tuning modification has little effect on frequency restoration. Moreover, the power sharing error eliminated with only local information is better than communication-based methods.

II. MOTIVATION

A. *Introduction of the primary control in cascaded type microgrid*

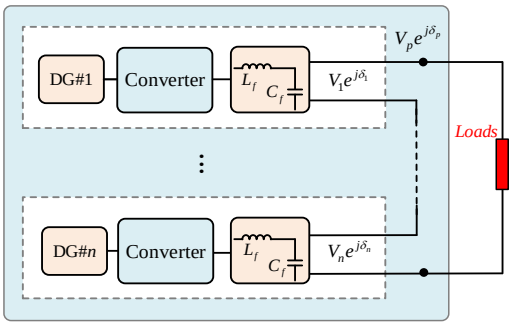

Fig. 2 Cascaded type microgrid configuration

Fig. 2 describes the configuration of a cascaded type microgrid comprised of *n* DGs. In this system, the interfacing converters are connected in series to achieve a high voltage. The voltage at the point of common coupling (PCC) equals the sum of all DG voltage vectors, which is expressed as follows

$$V_p e^{j\delta_p} = \sum_{i=1}^{n} V_i e^{j\delta_i} \tag{1}$$

where the output voltage of the *i-th* converter is denoted as

$V_i e^{j\delta_i}$ and the PCC voltage is represented by $V_p e^{j\delta_p}$.

According to [15, 23, 27, 28], the primary control for the cascaded microgrid is commonly designed as

$$\begin{cases} f_i = f^* + \mathrm{sgn}(Q_i) m_i P_i \\ V_i = \varphi(P_i^*) V^* \end{cases} \tag{2}$$

where f_i and V_i are the frequency and voltage amplitude references of the *i-th* DG unit, respectively. m_i is the primary control coefficient, which is designed to meet $m_i = |\Delta f_{\max}| / P_i^*$. The $|\Delta f_{\max}|$ is the maximum frequency deviation. The f^* represents the frequency reference value at no load. The V^* is the nominal voltage value of the cascaded microgrid. P_i^* is the nominal rated power of the *i-th* cascaded unit. The sgn(·) presents sign function, which is designed for extending stable region. The function $\varphi(\cdot)$ is expressed as follows

$$\mathrm{sgn}(x) = \begin{cases} 1 & x > 0 \\ 0 & x = 0 \\ -1 & x < 0 \end{cases} \tag{3}$$

$$\varphi(P_i^*) = P_i^* / P_{total}^* = P_i^* \Big/ \sum_{j=1}^{n} P_j^* \tag{4}$$

Generally, the nominal rated power of each unit can be acquired. So in practice, the expression $\varphi(P^*{}_i)$ is usually calculated offline, which does not rely on real-time communications.

B. The Motivation of Second Frequency Control for the Cascaded-type Microgrid

Although the primary control can achieve frequency synchronization and power sharing, the frequency deviation cannot be avoided. Fig. 3 represents the frequency/power curves under the primary control. When the system operates with RL load, the *f*/*P* curve is in the blue area and the frequency will increase in steady state. When the system operates with RC load, the primary response is different. As shown in the red area, the frequency will decrease in steady state. It can be seen that different load characteristics will lead to different system frequency variation trends. This is a unique characteristic for cascaded-type microgrid, which is quite different from the paralleled-type microgrid. To improve the power quality of the system, it is necessary to restore the frequency of the system.

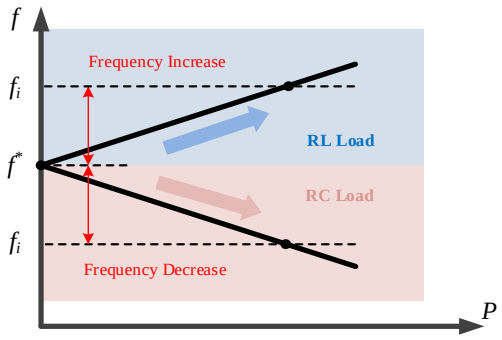

Fig. 3 Frequency/power curves under the primary control

In the proposed control, some disturbance will cause power sharing error, which can lead to the PCC voltage decrease. Due to the power-sharing error, the power factor angles of all DGs will not be consistent. As shown in Fig. 4, although the voltage amplitude of each DG unit does not change, the unbalanced power factor angle will decrease the PCC voltage amplitude according to the vector sum principle.

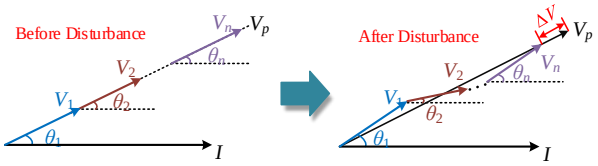

Fig. 4 Voltage drop mechanism with power-sharing error

III. Proposed Control Design

A. Second Frequency Control Design

To overcome the drawbacks, the objectives of the second control for the cascaded-type microgrid are to restore the frequency and obtain accurate average power sharing, which can be expressed as follows

$$\lim_{t\to\infty}\left(f^* - f_i\right) = 0, \quad i = 1, 2, \cdots n \tag{5}$$

$$\lim_{t\to\infty}\left(m_i P_i - m_j P_j\right) = 0, \quad i, j = 1, 2, \cdots n \,\&\, i \neq j \tag{6}$$

To achieve the aforementioned goals, this paper proposes a decentralized secondary control, which has two modifications based on the primary frequency control. One modification ψ_i is for restoring frequency and another modification ξ_i is to eliminate power sharing error

$$\begin{cases} f_i = f^* + g(Q_i)\left(m_i P_i + \xi_i\right) + \psi_i \\ \psi_i = \dfrac{k_{Ii}}{s}\left(f^* - f_I\right) \\ \xi_i = G_i \sum_{x=1}^{k-1}\left(m_i P_{i,x}\right)^{\gamma} \end{cases} \tag{7}$$

where k_I is the coefficient of the secondary controller. f_I is the output current frequency. G_i is the self-tuning coefficient. The index γ is the convergence rate coefficient. The frequency restoration is conducted by PI controller, and the self-tuning modification is a time-trigger control law, which is based on precise pulse per second (PPS). The two modifications work at different time scales. The sample period T_f of frequency modification ψ_i is the same as the primary control. The time interval T_s between k and $k+1$ self-tuning modification is much larger than T_f, which is set to 1s in this paper. The subscript x represents the *x-th* trigger. The diagram of g(Q) is shown Fig. 5. The switch will be enbled when the absolute value of Q_i larger than Q_{upper} and will be disable when the absolute value of Q_i less than Q_{lower}. In this paper, Q_{upper} =20Var and Q_{lower}=3Var are selected.

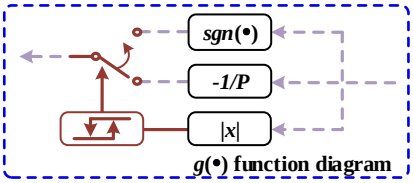

Fig. 5 Detail diagram of g(·).

B. Analysis of frequency restoration modification

As for cascaded-type microgrid, all DG units share the same load current, which is global information in nature. The proposed control adopts the nature characteristic to regulate the whole system frequency. The current angles δ_I are derived

as follow

$$\delta_I = a\tan\frac{\sum_{i=1}^{n}\varphi\left(P_i^*\right)\sin\left(\delta_i-\theta_{load}^{'}\right)}{\sum_{i=1}^{n}\varphi\left(P_i^*\right)\cos\left(\delta_i-\theta_{load}^{'}\right)} \tag{8}$$

$$Z_{load}^{'}e^{j\theta_{load}^{'}} = Z_{load}e^{j\theta_{load}} + Z_{line}e^{j\theta_{line}} \tag{9}$$

where $Z_{load}^{'}$ and $\theta_{load}^{'}$ are the amplitude and angle of the vector sum of line impedance $Z_{line}e^{j\theta_{line}}$ and load impedance $Z_{load}e^{j\theta_{load}}$.

Then, the current frequency can be calculated by derivation of (8)

$$f_I = \frac{1}{2\pi}\dot{\delta}_I = \frac{1}{2\pi}\sum_{i=1}^{n}\varphi\left(P_i^*\right)f_i \tag{10}$$

From (10), the output current frequency represents the weighted average frequency of all DG units. In steady state, all units share the same frequency and the frequency restoration is achieved due to the PI controller. The system frequency is restored to the reference value, which is expressed as follow

$$f_1 = f_2 = \cdots = f_n = f_I = f^* \tag{11}$$

To further illustrate the frequency restoration mechanism, Fig. 6 shows the *f*/*P* curves and operating point variation under frequency restoration modification. From Fig. 6, assume that point *a* is the initial state of the system under no load. When the system operates with RL load, the system frequency has increased and the operating point shifts from point *a* to *b*. After frequency restoration, the *f*/*P* curve moves downward and the operating point moves to point *c*. When the system operates with RC load, the operating point *a* moves to *b* along the original *f*/*P* curve, which is accompanied by a frequency decrease. Then, the frequency restoration can be regarded as an upward movement of the curve, whereas operating point *b* follows the curve with a vertical translation. Hence, frequency restoration can be achieved

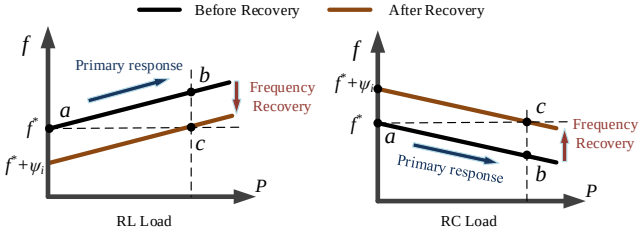

Fig. 6 Frequency restoration schematic diagram

C. Analysis of self-tuning modification

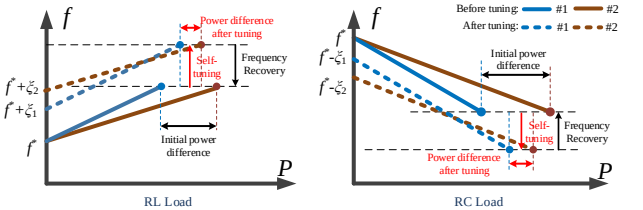

Fig.7 Example for self-tuning modification mechanism

Fig. 7 describes a specific example of two DG units with the same capacity connecting in series to explain the self-tuning modification mechanism. In the beginning, there is power sharing difference between the two DG units. The self-tuning modification is to make the *f*/*P* curve of each DG unit change according to its output power. In detail, the *f*/*P* curve of the DG with larger power will shift more than the *f*/*P* curve of the DG with less power. Thus, the mechanism behind the sharing error reduction is that the DG with larger power decreases its output power and the output power of the DG with less power will increase. If the self-tuning modification is repeated, their output power tends to be consistent, and the active power-sharing error will be eliminated eventually. Due to the same output current, the reactive power sharing is also achieved, which is discussed in [21~23, 27, 28]].

In addition, the frequency deviation caused by the self-tuning modification can be restored by the frequency restoration modification. Because the time scale of the self-tuning modification is much smaller than the time scale of the frequency restoration modification. That is to say, if the self-tuning modification leads to frequency deviation, then the frequency restoration will restore the system frequency to rating value in a short time before the next self-tuning modification trigger.

When the system works under pure resistance load, each unit of the system does not provide reactive power, which means that the value of Q_i is very small. At this time, the phase angles of output current and voltage are almost the same. Since the same sharing output current, the active power of each unit is proportional to the voltage amplitude. The voltage amplitude of each unit is designed according to its capacity, so the system can still keep active power sharing. So when the absolute value of Q_i is less than Q_{lower}, the self-tuning modification does not need to start.

$$P_1 : P_2 : \cdots : P_n = V_1 : V_2 : \cdots : V_n = P_1^* : P_2^* : \cdots : P_n^* \tag{12}$$

D. Synchronization clock based on Precise Pulse per Second

All the self-tuning modification is activated by the periodic PPS signal, which is shown in Fig. 8. Although there are still PPS errors, the effect of the proposed self-tuning modification will not be affected. Because the time interval T_s are much larger than the PPS error, which does not exceed 100ns. Besides, the errors do not accumulate, which will be eliminated by the frequency modification response. Moreover, the global synchronization clock is indispensable for system startup, protection, and grid connection, so this will not bring much additional cost.

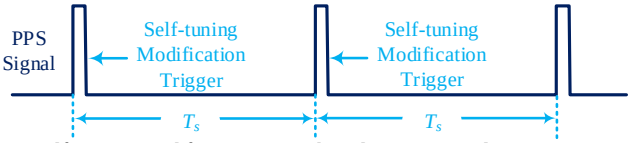

Fig. 8 Self-tuning modification trigger based on PPS signal

IV. Stability Analysis Based on Singular Perturbation Theory

According to singular perturbation theory, when analyzing the boundary layer system (reduced fast system), we can consider the slow variable as a constant value. Whereas, when focusing on the outer system (reduced slow system), the dynamic of the fast variable can be neglected [29]. Since the frequency restoration control and self-tuning modification are with two different time scales, we can analyze the stability of frequency restoration control and convergence of self-tuning modification separately.

A. Power Transmission Model

Based on the circuit theory, the power flows of the *i-th* DG units in the cascaded-type microgrid are obtained as

$$P_i = \frac{V_i}{|Z_{load}|}\sum_{j=1}^{n} V_j \cos\left(\delta_i + \theta'_{load} - \delta_j\right) \tag{13}$$

$$Q_i = \frac{V_i}{|Z_{load}|}\sum_{j=1}^{n} V_j \sin\left(\delta_i + \theta'_{load} - \delta_j\right) \tag{14}$$

By linearizing (13, 14) and moving the equilibrium points to the origin, the small-signal equations of the power transmission model are derived as

$$\Delta P_i = -\frac{V^{*2}}{|Z_{load}|}\varphi\left(P_i^*\right)\sin\theta'_{load}\sum_{j=1}^{n}\varphi\left(P_j^*\right)\left(\Delta\tilde{\delta}_i - \Delta\tilde{\delta}_j\right) \tag{15}$$

$$\Delta Q_i = \frac{V^{*2}}{|Z_{load}|}\varphi\left(P_i^*\right)\cos\theta'_{load}\sum_{j=1}^{n}\varphi\left(P_j^*\right)\left(\Delta\tilde{\delta}_i - \Delta\tilde{\delta}_j\right) \tag{16}$$

where $\tilde{\delta}_i = \delta_i - \delta_{is}$ and δ_{is} is the steady-state value of δ_i, which is defined as $\delta_{is}=\int 2\cdot\pi\cdot f^* \mathrm{d}t$

B. Analysis of the Boundary Layer System

On the fast time scale, we can analyze the stability of the restoration control by considering the self-tuning modification as a constant. Thus, calculate partial differential of (7) and we can obtain the small-signal equation of the boundary layer system dynamic model.

$$\frac{d\Delta f_i}{dt} = \begin{cases} \mathrm{sgn}\left(Q_{is}\right) m_i \dfrac{d\Delta P_i}{dt} - k_{Ii}\Delta f_I & |Q| \geq Q_{upper} \\ -m_i \dfrac{d\Delta Q_i}{dt} - k_{Ii}\Delta f_I & |Q| \leq Q_{lower} \end{cases} \tag{17}$$

Substitute (15, 16) and $m_i=|\Delta f_{\max}|/P_i^*$ to (15), we can obtain

$$\frac{d\Delta f_i}{dt} = -C_x\sum_{j=1}^{n} P_j^*\left(\Delta f_i - \Delta f_j\right) - k_{Ii}\sum_{j=1}^{n} P_j^*\Delta f_j \Big/ P_{total}^* \tag{18}$$

where

$$C_x = \begin{cases} C_1 = \mathrm{sgn}\left(Q_{is}\right)\dfrac{2\pi V^{*2}|\Delta f_{\max}|}{|Z_{load}|P_{total}^{*2}}\sin\theta'_{load} & |Q| \geq Q_{upper} \\ C_2 = \dfrac{2\pi V^{*2}|\Delta f_{\max}|}{|Z_{load}|P_{total}^{*2}}\cos\theta'_{load} & |Q| \leq Q_{lower} \end{cases} \tag{19}$$

Since sgn (Q_{is})= sgn (Q_{js})= sgn (Q_{load}) and $\cos\theta'_{load}>0$, C_x is always non-negative

According to the Lyapunov energy function method, if a given system can find a positive definite energy function $V(x)$ and satisfy $\dot{V}(x)<0$, the total energy of the system will gradually decrease and eventually reach a stable state. To introduce the Lyapunov function, the positive energy function is defined as follows

$$V = \frac{1}{2}\sum_{i=1}^{n} P_i^*\Delta f_i^{\,2} > 0 \tag{20}$$

The derivation of (20) is expressed as follow

$$\dot{V} = -C_x\sum_{i=1}^{n}\sum_{j=1}^{n} P_i^*P_j^*\left(\Delta f_i - \Delta f_j\right)^2 - \frac{1}{P_{total}^*}\left(\sum_{j=1}^{n} k_{Ij}P_j^*\Delta f_j\right)\left(\sum_{j=1}^{n} P_j^*\Delta f_j\right) \tag{21}$$

From (21), if $k_{I1}=k_{I2}=\ldots=k_{In}>0$, the derivation of energy function will be less than zero. According to the Lyapunov energy function method, the local asymptotic convergence of the boundary layer system is achieved. The larger the second control coefficient is, the transient energy decreases faster, which accelerates system frequency restoration.

C. Validation of the small signal model

To verify the validation of small signal model, the simulation tests of comparison between the small signal model and physical simulation model are conducted. The parameters are presented in Table II. When $|Q_i|\geq Q_{upper}$ as shown in Fig. 9(a), the same disturbance is added on the small signal model and the simulation model at t=4s, respectively. After disturbing, both small signal model and physical simulation model can return to the original steady state point. However, during the dynamic process, there exists errors between small signal model and physical simulation model. These errors are mainly introduced by the linearization process, which is inevitable. As observed in Fig. 9 (b), when $|Q_i|\leq Q_{lower}$, the results are similar to the case of $|Q_i|\geq Q_{upper}$. From the two simulation results, although there are some small errors, the small signal model responses are roughly consistent with the system responses.

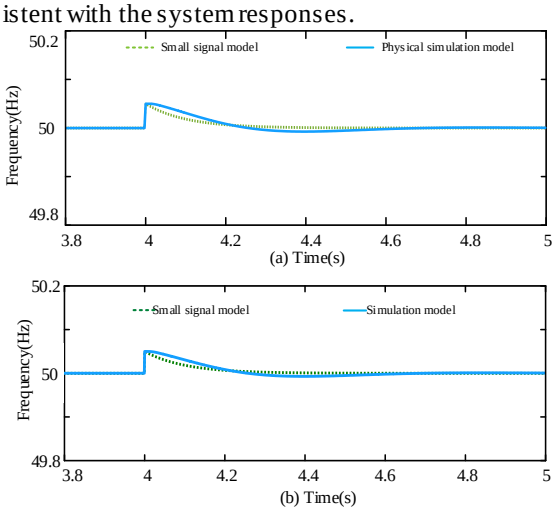

Fig. 9 Simulation test of comparison between the small signal model and physical simulation model: (a) $|Q_i|\geq Q_{upper}$, (b) $|Q_i|\leq Q_{lower}$,

D. Analysis of the Outer System

In this section, the convergence of the self-tuning modification is analyzed. When focusing on the slow time scale, the frequency is considered to be restored to the rated value. According to (7), the outer system models of the *i-th* DG and the *j-th* DG are derived as follow

$$0 = m_iP_{i,k} + G_i\sum_{x=1}^{k-1}\left(m_iP_{i,x}\right)^{\gamma} + \psi_{i,k} \tag{22}$$

$$0 = m_jP_{j,k} + G_j\sum_{x=1}^{k-1}\left(m_jP_{j,x}\right)^{\gamma} + \psi_{j,k} \tag{23}$$

Generally, the coefficient of self-tuning modification is set to be the same, which can be expressed as $G_i=G_j=G$. Subtracting the slow-scale model of the *j-th* DG from the slow-scale model of the *i-th* DG, then

$$m_iP_{i,k} - m_iP_{j,k} = e_{ij} - G\sum_{x=1}^{k-1}\left(\left(m_iP_{i,x}\right)^{\gamma} - \left(m_jP_{j,x}\right)^{\gamma}\right) \tag{24}$$

where e_{ij} represents the power sharing error accumulated by initial integral errors, disturbance on current frequency measurement, and frequency restoration integration. It is noted this power sharing error can be assumed as a constant to simplify the following analysis.

Define $m_iP_{i,k} \geq m_jP_{j,k} > 0$ and $Z_{ij,k} = m_iP_{i,k} - m_jP_{j,k}$, and then

$$Z_{ij,k} = e_{ij} - G\sum_{x=1}^{k-1}\left(\left(m_i P_{i,x}\right)^{\gamma} - \left(m_j P_{j,x}\right)^{\gamma}\right) \tag{25}$$

From (25), we can obtain a nonnegative sequence, which is derived as follow

$$\begin{cases} Z_{ij,k+1} = \left(1 - GS_{ij,k}\right) Z_{ij,k} \\ Z_{ij,1} = e_{ij} \end{cases} \tag{26}$$

where

$$S_{ij,k} = \sum_{y=0}^{\gamma-1}\left(\left(m_i P_{i,k}\right)^{y}\left(m_j P_{j,k}\right)^{\gamma-1-y}\right) \tag{27}$$

As $0 < m_i P_{i,k} \le m_i P_i^* = \Delta f_{\max}$, we can obtain

$$0 < S_{ij,k} \le \gamma \left|\Delta f_{\max}\right|^{\gamma-1} < 1 \tag{28}$$

If coefficients G and γ are set to satisfy $0 < G \cdot \gamma \cdot \Delta f_{\max}{}^{\gamma-1} < 1$, there exists a positive number ρ satisfying

$$0 < \max_{x=1}^{k}\left(1 - G \cdot S_{ij,x}\right) \le \rho < 1 \tag{29}$$

Substitute (29) to (26), then

$$Z_{ij,k+1} = \left(1 - GS_{ij,k}\right) Z_{ij,k} \le \rho Z_{ij,k} \le \rho^2 Z_{ij,k-1} \le \cdots \le \rho^k Z_{ij,1} \tag{30}$$

The right-hand side tends to zero as $k \to \infty$. Combining with the definition $Z_{ij,k+1} \ge 0$, we can obtain

$$0 \le Z_{ij,k+1} \le 0 \Rightarrow Z_{ij,k+1} = 0 \tag{31}$$

Obviously, the $Z_{ij,k+1}$ will converge to zero. In other words, the proposed control can achieve active power sharing eventually. In addition, larger coefficients G and γ can increase the convergence rate. But it is worth mentioning that very large G and γ will affect system convergence and lead to unallowable frequency fluctuation.

Thus, the selection of G and γ is very important, which should satisfy the following condition

$$\begin{cases} 0 < G \cdot \gamma \cdot \left|\Delta f_{\max}\right|^{\gamma-1} < 1 \\ G\left(m_i P_i\right)^{\gamma} \le G\left|\Delta f_{\max}\right|^{\gamma} = \left|\Delta f_f\right| \end{cases} \tag{32}$$

where $\left|\Delta f_f\right|$ is the maximum frequency fluctuation.

From the second equation of (32), the selection of G is derived as follow

$$G = \frac{\left|\Delta f_f\right|}{\left|\Delta f_{\max}\right|^{\gamma}} \tag{33}$$

Combining (32) and (33), the selection principle of convergence speed rate γ is derived as

$$0 < \gamma < \frac{\left|\Delta f_{\max}\right|}{\left|\Delta f_f\right|} \tag{34}$$

From (33) and (34), to acquire a fast convergence rate, the coefficients G and γ are selected as large as possible within the derived range above.

V. Real-time Simulation Results

In this part, the real-time simulation tests with selecting a cascaded-type microgrid comprised of four cascaded units are carried out based on RT-LAB OP4510. The topology of the system and the detailed control diagram are presented in Fig. 10. The parameters of the simulated system are listed in Table II.

TABLE II
Simulation Parameters

Symbol	Item	Value
V^*/f_{ref}	Voltage reference	311 V/50 Hz
$P^*_{\max}$	Rated power	1 kW
$\Delta f_{\max}$	Max frequency deviation	±0.5 Hz
Δf_f	Max frequency fluctuation	±0.1Hz
m	Control coefficient	5e-4
k_I	Frequency restoration coefficient	4
G	Self-tuning coefficient	1.6
γ	Convergence rate coefficient	4
L_f	Filter inductance	0.6mH
C_f	Filter capacitor	20uF

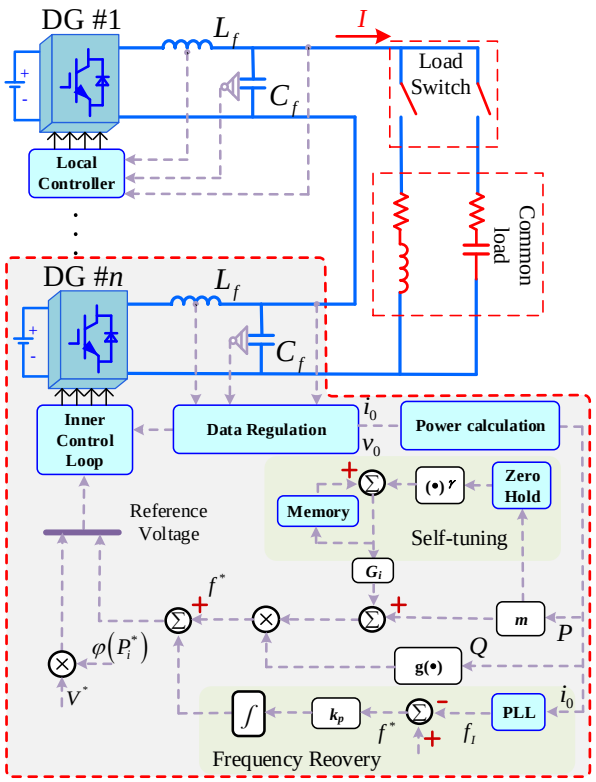

Fig. 10 Proposed control diagram.

A. Case I: Feasibility of frequency restoration under different types of load

In this part, only frequency restoration modification is conducted. Fig. 11 (a) and Fig. 11 (b) represent the simulation results of the control strategy with resistive-inductive and resistive-capacitive loads, respectively. When under RL load, in the beginning, the cascaded-type microgrid operates under primary control and the frequency deviation is visible. After frequency restoration modification starting (t=2s), frequency restoration is achieved eventually. During the dynamic process, the adjustment time is less than 1s and the overshoot peak value is small. Thus, the transient performance and dynamic response of output power are satisfied. At t=4s, a load step up change occurs. After a brief fluctuation, the frequency returns to 50Hz again and the power sharing has not been affected. When with RC load the dynamic process is similar to the case with RL loads, and the frequency restoration and power sharing are achieved in steady state. To avoid repetition, the results will not be discussed in detail. The effectiveness of the proposed control method for frequency restoration is verified and the stability is

This article has been accepted for publication in IEEE Transactions on Power Systems. This is the author's version which has not been fully edited and content may change prior to final publication. Citation information: DOI 10.1109/TPWRS.2022.3206341

insensitive to load impedance characteristics.

B. *Case II: Feasibility of frequency restoration under different types of load*

Fig. 12 shows the simulation test results under pure R load and load characteristic change. In this test, the system starts to work under pure resistance load. A load of R=30Ω is added at t=2s. The results show that the proposed control can work well under pure resistance load. In addition, the load characteristic is changed from R to RL and RL to RC at t=4s and t=6s, respectively. After load characteristic change, the dynamic performance of active power and reactive power is satisfactory. Although the characteristic change will bring frequency fluctuation, the frequency overshoot is still within the allowable range. In steady state, frequency restoration and power sharing are ensured. All in all, the results show the effectiveness of the proposed control under pure R load and load characteristic change.

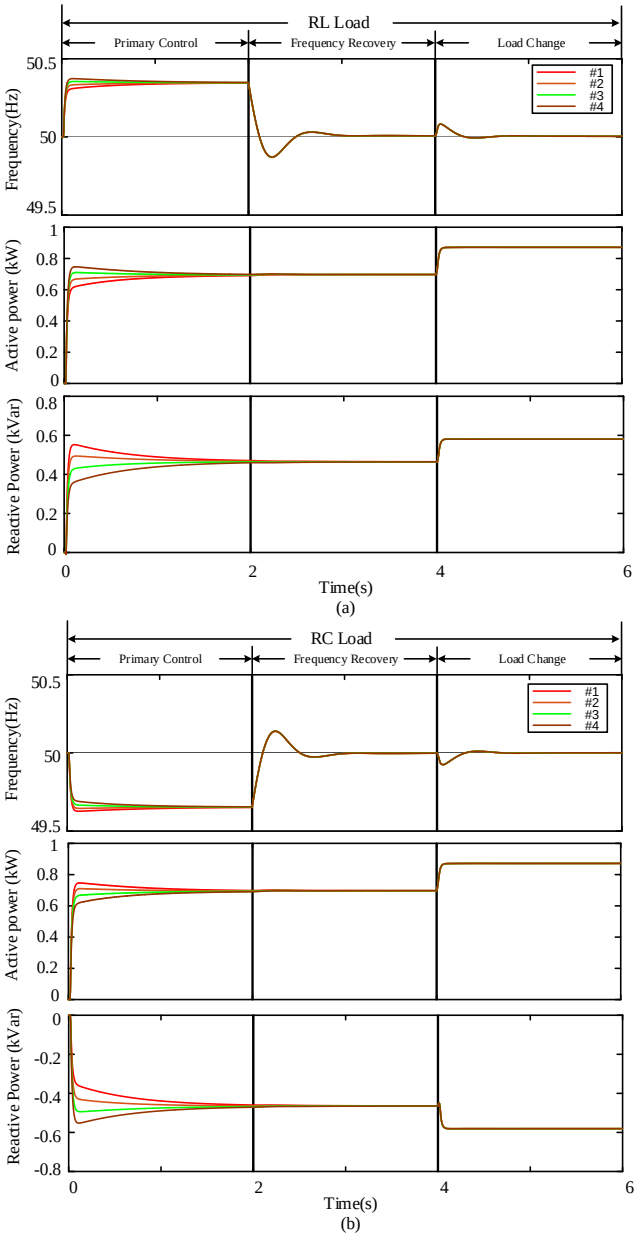

Fig.11 Simulation results of frequency recovery verification: (a) with RL load, (b) with RC load

C. *Case III: Feasibility of frequency restoration under pure R load with phase error*

In this section, a simulation test of the proposed control under pure R load is carried out. The RL load and R load are selected as 20+12jΩ and 25Ω, respectively. At t=2s, the load is changed from RL load to R load. As shown in Fig. 13, after load changing, although the control change will bring frequency fluctuation, the frequency synchronization and restoration are achieved eventually. Moreover, to verify the robustness of the proposed method under pure R load, different phase errors for each unit occur at t=4s. After phase errors occurring, the frequencies of each unit are disturbed. Under proposed control, the frequency disturbance is eliminated and the frequency synchronization and restoration are still guaranteed.

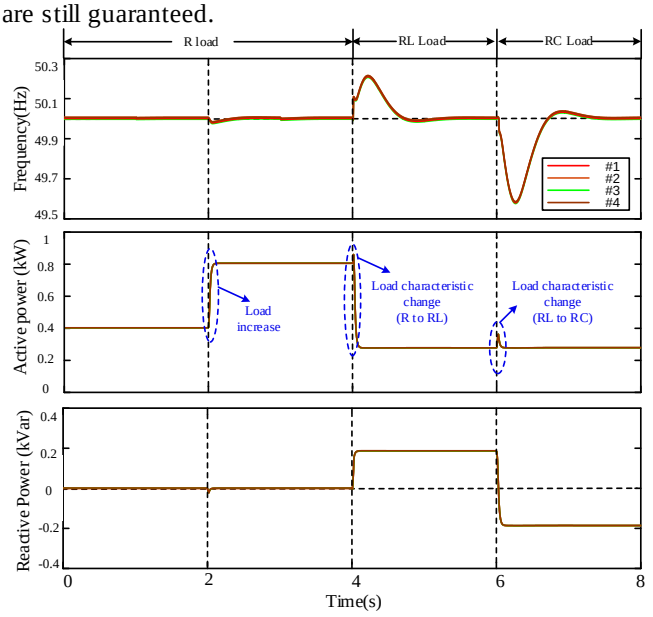

Fig. 12 Simulation results of the control performance under load characteristic change.

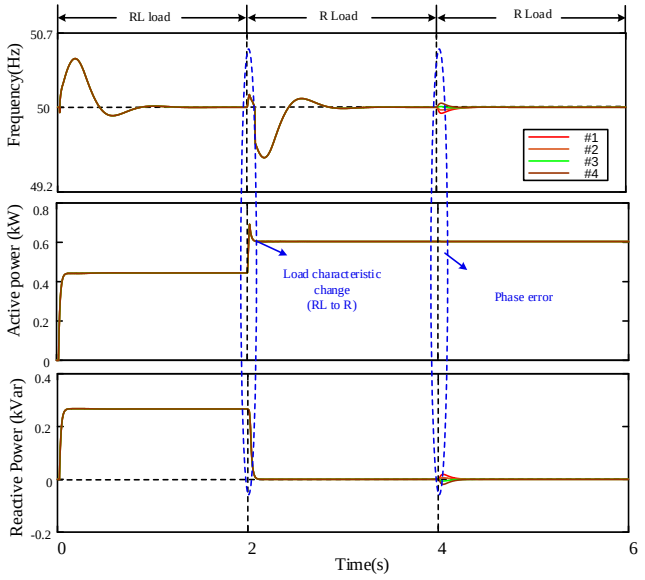

Fig.13 Simulation results of the control performance under pure R load with phase error

D. *Case IV: Feasibility of self-tuning modification.*

To better verify the feasibility of self-tuning modification, we add a random error at t=2s. As observed in Fig. 14, although the frequency restoration can be achieved after

This article has been accepted for publication in IEEE Transactions on Power Systems. This is the author's version which has not been fully edited and content may change prior to final publication. Citation information: DOI 10.1109/TPWRS.2022.3206341

fluctuation, the power sharing among each unit cannot be maintained. When the proposed modification starts at t=4, the self-tuning modification starts to regulate the power outputs, thereby output power errors of all units decrease step by step. Moreover, load change does not affect the power sharing performance and a fast dynamic response can be obtained. In steady state, the frequency is restored to the normal value (50Hz) and the power-sharing accuracy is improved. Although there are still small and transient fluctuations when the modification triggers, the fluctuations are within the acceptable range during the whole adjustment process. All in all, the feasibility of self-tuning modification is verified.

E. Case V: Influence of coefficient γ on convergence speed.

This case is to discuss the influence of coefficient γ on convergence speed through simulation tests. Three different groups of self-tuning modification coefficients are selected: 1. G=1.6 and γ=4; 2. G=0.4 and γ=2; 3. G=0.2 and γ=1. From the three test results in Fig. 15, the coefficient group 3 can achieve the fastest convergence speed compared to the other two groups. We can conclude that the greater the γ, the faster the convergence speed, which is the same as the above theoretical analysis.

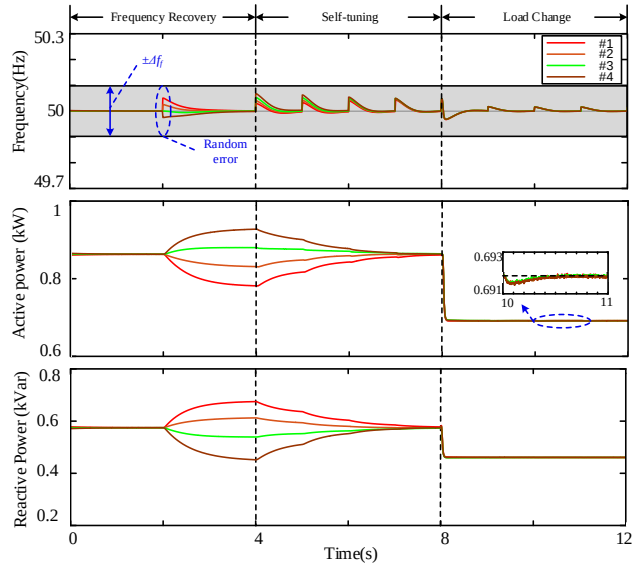

Fig. 14 Simulation results of self-tuning modification verification.

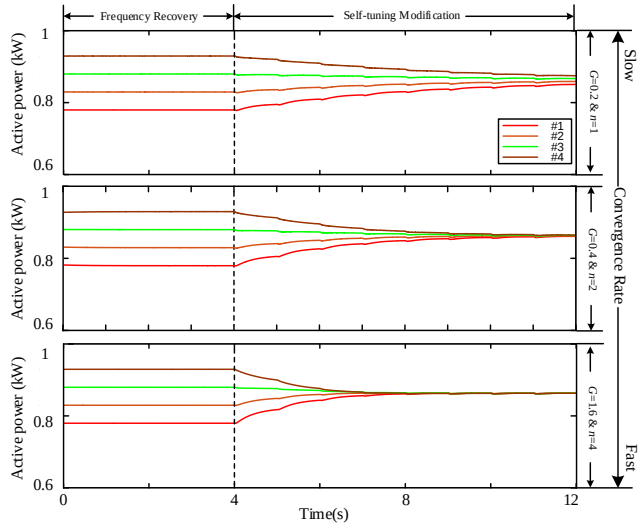

Fig.15 Simulation results of the control performance with different γ and G.

F. Case VI: Influence of PPS errors on control effect

In this section, we aim to explore the impact of normal PPS errors on the control effect. Generally, the accuracy of PPS can reach 100ns. To better prove that the PPS error has little effect on the control effect, the error conducted in this case is 100 times larger than the normal. The PPS error is randomly generated between 0 and 10ms. As observed from the enlarged view of the correction trigger (t=2) in Fig. 16, the maximum PPS error reached 10ms. However, the output power of each DG can also keep the convergence trend and achieve balance in steady state. As observed from the enlarged view of output power (t=10), the maximum power-sharing error is less than 1 w, which is within the allowable range. Moreover, the power distribution returns into a balanced state before the next PPS signal triggering. Thus, the proposed method has good fault tolerance for normal PPS errors.

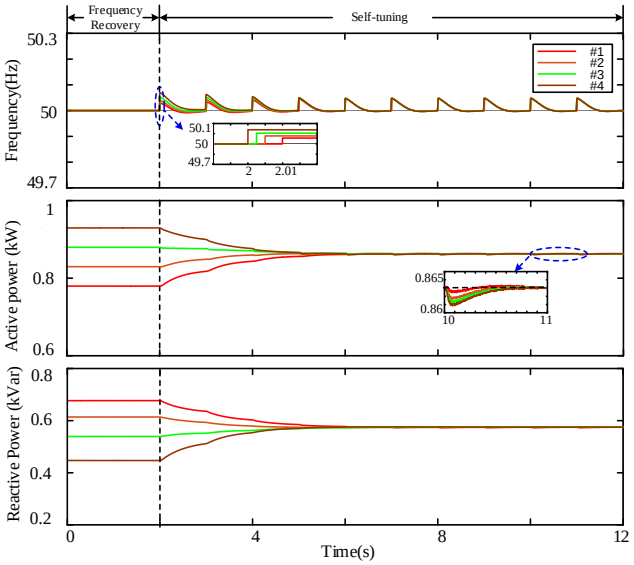

Fig.16 Simulation results of the control performance with PPS errors.

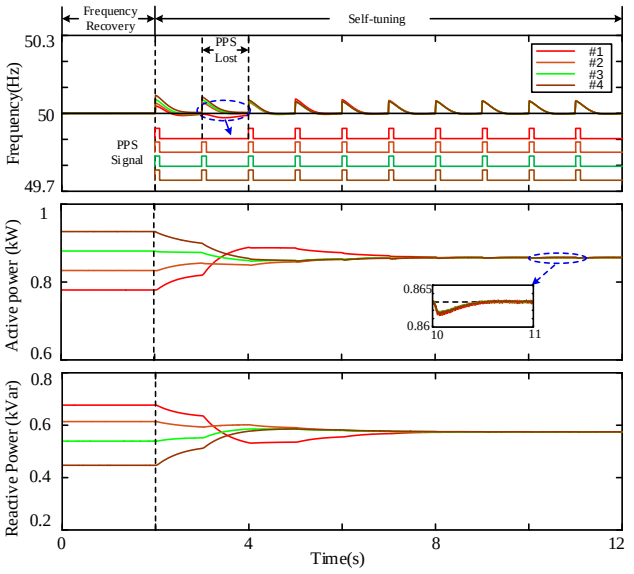

Fig.17 Simulation results of the control performance with transient PPS signal loss.

G. Case VII: Influence of PPS lost on control effect

In this case, the PPS signal that the #1 DG received is lost during the period of t=3~4s. When the PPS signal of #1 DG

is lost, the active power of the #1 DG no longer maintains the convergence trend, which is different from the output power of the other three DGs. It can be seen from Fig. 17, when the PPS signal is restored, the active power of the #1 DG keeps the converged again and the power sharing is achieved in steady state. The steady-state performance is the same as that without PPS signal loss. It is noted that the long-term PPS signal loss is still unacceptable, which will decrease the control performance. If the PPS signal is lost for a long time, the entire self-tuning modification needs to be stopped triggering.

VI. CONCLUSION

In this paper, a decentralized secondary control method is proposed for the cascaded-type microgrid. Combined with the characteristics of the series structure, the frequency recovery modification can be easily designed by using the global average frequency acquired from the sharing output current. In addition, a self-tuning modification is proposed to improve power sharing accuracy. Since real-time communication is not required, the threat of communication disturbance is decreased, which also increases system reliability to a certain extent. Moreover, the stability has been proved based on singular perturbations theory and the simulation tests based on RTLAB have validated the feasibility of the proposed control method.

REFERENCES

[1] A. Ipakchi and F. Albuyeh, "Grid of the future," IEEE Power and Energy Magazine, vol. 7, no. 2, pp. 52–62, Mar. 2009.

[2] X. Yu and Y. Xue, "Smart Grids : A Cyber–Physical Systems Perspective," Proceedings of the IEEE, vol. 104, no. 5, May 2016.

[3] J. M. Guerrero, L. G. de Vicuna, J. Matas, M. Castilla, and J. Miret, "A Wireless Controller to Enhance Dynamic Performance of Parallel Inverters in Distributed Generation Systems," IEEE Transactions on Power Electronics, vol. 19, no. 5, pp. 1205–1213, Sept. 2004.

[4] J. M. Carrasco, L. G. Franquelo, J. T. Bialasiewicz, E. Galván, R. C. P. Guisado, M. ´ Angeles, M. Prats, J. I. León, and N. Moreno-alfonso, "Power-Electronic Systems for the Grid Integration of Renewable Energy Sources : A Survey," vol. 53, no. 4, pp. 1002–1016, Aug. 2006.

[5] X. Lu, K. Sun, J. M. Guerrero, J. C. Vásquez, and L. Huang, "State-of-Charge Balance Using Adaptive Droop Control for Distributed Energy Storage Systems in DC Microgrid Applications," IEEE Transactions on Industrial Electronics, vol. 61, no. 6, pp. 2804–2815, June 2014.

[6] J. M. Guerrero, J. C. V´asquez, J. Matas, M. Castilla, L. G. D. Vicu˜na, and M. Castilla, "Hierarchical control of droop-controlled AC and DC microgrids—A general approach toward standardization," IEEE Transactions on Industrial Electronics, vol. 58, no. 1, pp. 158–172, Jan. 2011.

[7] J. A. P. Lopes, C. L. Moreira, and A. G. Madureira, "Defining control strategies for microgrids islanded operation," IEEE Transactions on Power Systems, vol. 21, no. 2, pp. 916–924, May 2006.

[8] A. Moradi Amani, N. Gaeini, M. Jalili and X. Yu, "Which Generation Unit Should be Selected as Control Leader in Secondary Frequency Control of Microgrids?," in IEEE Journal on Emerging and Selected Topics in Circuits and Systems, vol. 7, no. 3, pp. 393-402, Sept. 2017

[9] Z. Shuai, W. Huang, X. Shen, Y. Li, X. Zhang and Z. J. Shen, "A Maximum Power Loading Factor (MPLF) Control Strategy for Distributed Secondary Frequency Regulation of Islanded Microgrid," in IEEE Transactions on Power Electronics, vol. 34, no. 3, pp. 2275-2291, March 2019.

[10] F. Guo, C. Wen, J. Mao and Y. D. Song, "Distributed Secondary Voltage and Frequency Restoration Control of Droop-Controlled Inverter-Based Microgrids," IEEE Transactions on Industrial Electronics, vol. 62, no. 7, pp. 4355-4364, Jul. 2015

[11] J. W. Simpson-Porco, Q. Shafiee, F. Dörfler, J. C. Vasquez, J. M. Guerrero and F. Bullo, "Secondary Frequency and Voltage Control of Islanded Microgrids via Distributed Averaging," in IEEE Transactions on Industrial Electronics, vol. 62, no. 11, pp. 7025-7038, Nov. 2015

[12] H. Xin, R. Zhao, L. Zhang, Z. Wang, K. P. Wong, and W. Wei, "A decentralized hierarchical control structure and self-optimizing control strategy for F-P type DGs in islanded microgrids," IEEE Transactions on Smart Grid, vol. 7, no. 1, pp. 3–5, Jan. 2016.

[13] H. Xin, L. Zhang, Z. Wang, D. Gan and K. P. Wong, "Control of Island AC Microgrids Using a Fully Distributed Approach," IEEE Transactions on Smart Grid, vol. 6, no. 2, pp. 943-945, March 2015.

[14] Xiaochao Hou, Yao Sun*, Hua Han, Zhangjie Liu, Wenbin Yuan, Mei Su."A Fully Decentralized Control of Grid-Connected Cascaded Inverters," IEEE Transactions on Sustainable Energy , vol.10, no.1, pp. 315-317, 2019.

[15] Guangze Shi, Hua Han, Yao Sun, Zhangjie Liu, Minghui Zheng and Xiaochao Hou "A Decentralized SOC Balancing Method for Cascaded-type Energy Storage System," IEEE Transactions on Industrial Electronics, early access, 2020

[16] P. Wu, Y. Su, J. -. Shie and P. Cheng, "A Distributed Control Technique for the Multilevel Cascaded Converter," in IEEE Transactions on Industry Applications, vol. 55, no. 2, pp. 1649-1657, March-April 2019, doi: 10.1109/TIA.2018.2876431.

[17] P. W. Hammond, "A new approach to enhance power quality for medium voltage ac drives," IEEE Trans. Ind. Appl., vol. 33, no. 1, pp. 202–208, Jan./Feb. 1997.

[18] R. H. Osman, "A medium-voltage drive utilizing series-cell multilevel topology for outstanding power quality," in Conf. Rec. IEEE IAS Annu. Meet., 1999, vol. 4, pp. 2662–2669.

[19] H. Akagi, S. Inoue, and T. Yoshii, "Control and performance of a transformerless cascade PWM STATCOM with star configuration," IEEE Trans. Ind. Appl., vol. 43, no. 4, pp. 1041–1049, Jul./Aug.2007

[20] J. He; Y. Li; B. Liang; C. Wang, "Inverse Power Factor Droop Control for Decentralized Power Sharing in Series-Connected Micro-Converters Based Islanding Microgrids," IEEE Trans. Industrial Electronics Early Access, Feb. 2017.

[21] Yao Sun, Guangze Shi, Xing Li, Wenbin Yuan, Mei Su, Hua Han, Xiaochao Hou."An f-P/Q Droop Control in Cascaded-type Microgrid," IEEE Transactions on Power Systems, vol.33, no.1 , pp. 1136-1138,Jan. 2018

[22] Yao Sun, Lang Li, Guangze Shi, Xiaochao Hou and Mei Su, "Power Factor Angle Droop Control—A General Decentralized Control of Cascaded Inverters," IEEE Transactions on Power Delivery ,vol. 36, no. 1, pp. 465-468, Feb. 2021.

[23] Lang Li, Yao Sun, Mei Su, Siqi Fu, "Decentralized Mutual Damping Control of Cascaded-type VSGs for Power and Frequency Oscillation Suppression," IEEE Transactions on Industrial Electronics, early access.

[24] J. He, X. Liu, C. Mu and C. Wang, "Hierarchical Control of Series-Connected String Converter-Based Islanded Electrical Power System," in IEEE Transactions on Power Electronics, vol. 35, no. 1, pp. 359-372, Jan. 2020

[25] J. He, Y. Liu and Y. Wang, "Cascaded Droop and Inverse Droop Regulation for Two-Layer Coordinated Power Flow Control in Series-Connected Power Cells," in IEEE Transactions on Industrial Electronics, vol. 68, no. 8, pp. 6939-6951, Aug. 2021.

[26] G. Shi, H. Han, Y. Liu, M. Su, Z. Liu and Y. Sun, "A Common Second Frequency Control of Island Cascaded-type Microgrid," 2019 IEEE Energy Conversion Congress and Exposition (ECCE), 2019, pp. 5407-5410.

[27] Lang Li, Yao Sun , Hua Han, Xiaochao Hou, Xufeng Yuan, Wei Xiong and Mei Su, "Communication-free optimal economical dispatch scheme for cascaded-type microgrids with capacity constraints," IET Power Electronics, vol. 13, no. 13, pp. 2866-2873, Oct. 2020.

[28] Lang Li, Yao sun, Hua Han, Xiaochao Hou, Mei Su, Zhangjie Liu."Power Factor Angle Consistency Control for Decentralized Power Sharing in Cascaded-type Microgrid," IET Generation, Transmission & Distribution, vol. 13, no. 6, pp. 850-857, Mar. 2019.

[29] A. Narang-Siddarth and J. Valasek, Nonlinear Time Scale System in Standard and Nonstandard Forms: Analysis and Control. Society for Industrial and Applied Mathematics, 2014.